Available online at www.sciencedirect.com
SCIENCE DIRECT®
Composites: Part B 35 (2004) 685–697
composites Part B: engineering
www.elsevier.com/locate/compositesb

Static and dynamic deformations of thick functionally graded elastic plates by using higher-order shear and normal deformable plate theory and meshless local Petrov–Galerkin method

L.F. Qian[a,1], R.C. Batra[b,*], L.M. Chen[a]

[a]Nanjing University of Science and Technology, Nanjing 210094, China
[b]Department of Engineering Science and Mechanics, Virginia Polytechnic Institute and State University, MC 0219, Blacksburg, VA 24061, USA

Received 4 June 2003; accepted 4 February 2004
Available online 15 April 2004

Abstract

Static deformations, and free and forced vibrations of a thick rectangular functionally graded elastic plate are analyzed by using a higher-order shear and normal deformable plate theory (HOSNDPT) and a meshless local Petrov–Galerkin (MLPG) method. All components of the stress tensor are computed from equations of the plate theory. The plate material, made of two isotropic constituents, is assumed to be macroscopically isotropic with material properties varying in the thickness direction only. Effective material moduli are computed by using the Mori–Tanaka homogenization technique. Computed results for static and free vibration problems are found to agree well with their analytical solutions. The response of the plate to impulse loads is also computed for different volume fractions of the two constituents. Contributions of the work include the use of the HOSNDPT and the MLPG method for the analysis of functionally graded plates.
© 2004 Elsevier Ltd. All rights reserved.

Keywords: Natural frequencies

1. Introduction

An advantage of functionally graded materials (FGMs) over laminated composites is that material properties vary continuously in an FGM as opposed to being discontinuous across adjoining layers in laminated composites. The variation of material properties in an FGM is usually obtained by changing the volume fractions of two or more compatible constituents. FGMs with material properties varying in the thickness direction can be manufactured by high speed centrifugal casting [1,2], or by depositing ceramic layers on a metallic substrate [3,4], and those with properties changing in the plane of a sheet by ultraviolet irradiation to alter the chemical composition [5]. A directed oxidation technique has been employed by Breval et al. [6] and Manor et al. [7] to deposit a ceramic layer on the outside surface. Functionally graded fiber reinforced composites can be manufactured by varying the volume fraction and/or the orientation of fibers in the preform prior to infusing resin into it.

Several authors [8–12] have used either a first-order or a third-order shear deformation plate theory coupled with the finite element method (FEM) to analyze deformations of FG plates. These plate theories neglect transverse normal deformations, and generally assume that a plane stress state of deformation prevails in the plate. These assumptions may be appropriate for thin plates, but may not give good results for thick plates with length/thickness equal to 5 or less. For example, a three-dimensional analytic solution by Vel and Batra [13,14] of thermoelastic deformations of an Al/SiC plate gave noticeable changes in the plate thickness. Jin and Batra [15–17], amongst others, have used the quasi-static two-dimensional linear thermoelasticity theory to study fracture characteristics at a crack tip in a FG plate; Vel and Batra [13] have used the same theory to analyze transient thermal stresses in a FG plate. Here, we study a mechanical problem and use a higher order shear and normal deformable plate theory (HOSNDPT) of Batra and Vidoli [18] to analyze static deformations, and free

* Corresponding author. Tel.: +1-540-231-6051; fax: +1-540-231-4574.
E-mail address: rbatra@vt.edu (R.C. Batra).
[1] Presently Visiting Scholar at Virginia Polytechnic Institute and State University.

1359-8368/$ - see front matter © 2004 Elsevier Ltd. All rights reserved.
doi:10.1016/j.compositesb.2004.02.004

and forced vibrations of a FG plate with a meshless local Petrov–Galerkin (MLPG) method [19,20].

In the HOSNDPT the three components of displacement are expanded in the thickness direction and terms up to the same degree in the thickness coordinate are retained. In the compatible HOSNDPT, three-dimensional Hooke's law is used to derive constitutive relations for various kinetic variables in terms of the kinematic variables. Transverse shear and normal stresses at a point are computed from the plate equations rather than by integrating, through the thickness, the three-dimensional balance of linear momentum. The compatible HOSNDPT has been successfully used to delineate static deformations, and free and forced vibrations of thick homogeneous elastic plates [21,22]. In the mixed HOSNDPT [18,23] constitutive relations, independent of the expansions of the kinematic variables, are postulated that satisfy traction boundary conditions on the top and the bottom surfaces of the plate. For the same order of the plate theory, the mixed HOSNDPT gives values of transverse normal and transverse shear stresses that are closer to their analytical values than the compatible HOSNDPT. However, the latter is easier to implement in a computer code.

The FG plate is assumed to be made of two randomly interspread isotropic constituents and the macroscopic response of the composite is taken to be isotropic. Effective elastic moduli of the composite are obtained by using the Mori–Tanaka method [24]. The goal here is to demonstrate that the compatible HOSNDPT and the MLPG method for thick FG plates give results very close to the analytical solution of a problem. Thus the technique of homogenizing material properties is less critical.

Meshless methods such as the element-free Galerkin [25], hp-clouds [26], the reproducing kernel particle [27], the smooth particle hydrodynamics [28], the diffuse element [29], the partition of unity finite element [30], the natural element [31], meshless Galerkin methods using radial basis functions [32], the modified smoothed particle hydrodynamics [53], and the meshless local Petrov–Galerkin (MLPG) [19,20] for finding an approximate solution of a given initial-boundary-value problem have gained popularity because nodes can be placed at arbitrary locations.

An advantage of the MLPG method [19,20] over the FEM and most of the other meshless methods is that no background mesh is required to numerically evaluate various integrals appearing in the local Petrov–Galerkin approximation of a given initial-boundary-value problem. The essential boundary conditions are satisfied either by using the penalty method or the method of Lagrange multipliers or by modifying the stiffness matrix and the load vector to eliminate the prescribed degrees of freedom. The MLPG method has been successfully used to study two-dimensional elastostatic and elastodynamic problems [33,34], convection dominated flows [35], deformations of homogeneous plates and free and forced vibrations of a homogeneous and isotropic plate [22,37,38] static and dynamic thermoelastic deformations [54,55], and vibrations of FG plates [56].

The paper is organized as follows. Section 2 gives the formulation of the problem including a brief description of the compatible HOSNDPT and the MLPG method. Results for an aluminum/zirconia plate loaded either statically or dynamically are given in Section 3. Results of the static analysis and computed natural frequencies of a simply supported square plate are found to match well with the corresponding analytical values. Conclusions are summarized in Section 4.

2. Formulation of the problem

2.1. Brief review of the compatible HOSNDPT

A schematic sketch of the problem studied and the rectangular Cartesian coordinate axes used to describe deformations of the rectangular plate are shown in Fig. 1. It is assumed that the plate occupies the region $\Omega = [0,a]\times[0,b]\times[-h/2,h/2]$ in the unstressed reference configuration. The midsurface of the plate is denoted by S, the boundary of S by Γ, and displacements of a point along the x,y and z-axes by u,v and w, respectively. Let $L_i(z)$, $i=1,2,\ldots$ be orthonormalized Legendre polynomials defined on $[-h/2,h/2]$. That is

$$\int_{-h/2}^{h/2} L_i(z)L_j(z)\mathrm{d}z = \delta_{ij}, \tag{1}$$

where δ_{ij} is the Kronecker delta. $L_0(z)$ is a constant, and $L_i(z)$ is a polynomial of degree i in z/h. Expressions for the orthonormal Legendre polynomials are given in Refs. [18,23]. By using the Legendre polynomials as basis functions, we expand u,v and w as power series in z to get

$$\mathbf{u}(x,y,z,t) = \begin{Bmatrix} u(x,y,z,t) \\ v(x,y,z,t) \\ w(x,y,z,t) \end{Bmatrix} = \sum_{i=0}^{K} \begin{Bmatrix} u_i(x,y,t) \\ v_i(x,y,t) \\ w_i(x,y,t) \end{Bmatrix} L_i(z). \tag{2}$$

Expansions (2) for displacements have been employed by Mindlin and Medick [39], Batra and Vidoli [18], and Batra et al. [23]. For $K \geq 2$, the plate theory is called higher-order. Terms up to the same degree in z are retained in the expansions (2) of the three components of displacement. Batra et al. [23] have studied the decay rate of different terms in Eq. (2) with the distance from a point source which gives the relative importance of

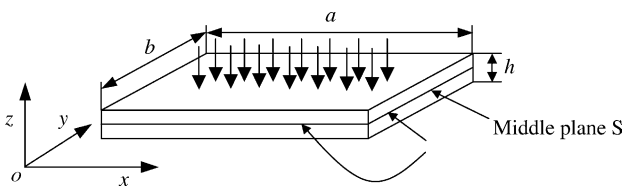

Fig. 1. Schematic sketch of the problem studied.

different terms. $L_i(z)$ has dimensions of (length)$^{-1/2}$ and u_i, v_i and w_i have dimensions of (length)$^{3/2}$. Recall that $L_i'(z) = \mathrm{d}L_i/\mathrm{d}z$ is a polynomial in z of degree $(i-1)$; thus it can be written as

$$L_i'(z) = \sum_{j=0}^{K} d_{ij} L_j(z), \tag{3}$$

where for a fixed h, d_{ij} are constants. Note that $d_{iK} = d_{Ki} = 0$ for $i = 0, 1, 2, \ldots, K$. Values of d_{ij} are computed by multiplying both sides of Eq. (3) with $L_k(z)$ and integrating the resulting equation with respect to z from $-h/2$ to $h/2$; these are listed in Refs. [18,23].

For infinitesimal deformations, the strain tensor $\boldsymbol{\varepsilon}$ is related to displacements (2) as follows:

$$\boldsymbol{\varepsilon} = \begin{Bmatrix} \varepsilon_{xx} \\ \varepsilon_{yy} \\ \varepsilon_{zz} \\ 2\varepsilon_{yz} \\ 2\varepsilon_{zx} \\ 2\varepsilon_{xy} \end{Bmatrix} = \sum_{i=0}^{K} \begin{Bmatrix} \dfrac{\partial u_i(x,y)}{\partial x} \\ \dfrac{\partial v_i(x,y)}{\partial y} \\ \displaystyle\sum_{j=0}^{K} w_j(x,y) d_{ji} \\ \dfrac{\partial w_i(x,y)}{\partial y} + \displaystyle\sum_{j=0}^{K} v_j(x,y) d_{ji} \\ \dfrac{\partial w_i(x,y)}{\partial x} + \displaystyle\sum_{j=0}^{K} u_j(x,y) d_{ji} \\ \dfrac{\partial v_i(x,y)}{\partial x} + \dfrac{\partial u_i(x,y)}{\partial y} \end{Bmatrix} L_i(z) \equiv \sum_{i=0}^{K} \{\eta_i\} L_i(z). \tag{4}$$

For $i = 0, 1, 2, \ldots, K$, $\boldsymbol{\eta}_i$ is a six-dimensional vector with components

$$\begin{aligned} &\eta_{i(1)} = \partial u_i/\partial x, \quad \eta_{i(2)} = \partial v_i/\partial y, \quad \eta_{i(3)} = \sum_{j=0}^{K} d_{ji} w_j, \\ &\eta_{i(4)} = \partial w_i/\partial y + \sum_{j=0}^{K} v_j d_{ji}, \quad \eta_{i(5)} = \partial w_i/\partial x + \sum_{j=0}^{K} u_j d_{ji}, \\ &\eta_{i(6)} = \partial v_i/\partial x + \partial u_i/\partial y. \end{aligned} \tag{5}$$

For $K > 1$, the transverse normal and the transverse shear strains depend upon $u_0, v_0, w_0, u_1, v_1, w_1, \ldots, u_{K-1}, v_{K-1}, w_{K-1}$. For an initially stress-free body, stresses $\boldsymbol{\sigma}$ at a point $\mathbf{x} = (x, y, z)$ are related to strains $\boldsymbol{\varepsilon}$ by Hooke's law:

$$\boldsymbol{\sigma} = \{\, \sigma_{xx} \quad \sigma_{yy} \quad \sigma_{zz} \quad \sigma_{yz} \quad \sigma_{zx} \quad \sigma_{xy} \,\}^{\mathrm{T}} = \mathbf{D}\boldsymbol{\varepsilon}. \tag{6}$$

Here, $\mathbf{D}$, the matrix of elastic constants, is a function of z. Substitution from Eq. (4) into Eq. (6) gives stresses at the point $\mathbf{x}$ in terms of displacements and in-plane gradients of displacements evaluated at the point (x, y) of the midsurface S.

Eq. (2) gives the following for the velocity $\dot{\mathbf{u}} = \partial \mathbf{u}/\partial t$ of a point:

$$\dot{\mathbf{u}}(x,y,z,t) = \begin{Bmatrix} \dot{u}(x,y,z,t) \\ \dot{v}(x,y,z,t) \\ \dot{w}(x,y,z,t) \end{Bmatrix} = \sum_{i=0}^{K} \begin{Bmatrix} \dot{u}_i(x,y,t) \\ \dot{v}_i(x,y,t) \\ \dot{w}_i(x,y,t) \end{Bmatrix} L_i(z). \tag{7}$$

A similar expression holds for the acceleration $\ddot{\mathbf{u}}$. If the initial velocity $\ddot{\mathbf{u}}(x, y, z, 0)$ is known then

$$\dot{u}_i(x,y,0) = \int_{-h/2}^{h/2} \dot{u}(x,y,z,0) L_i(z)\,\mathrm{d}z, \tag{8}$$

and similar expressions hold for $\dot{v}_i(x, y, 0)$, $\dot{w}_i(x, y, 0)$ and the initial displacement $\mathbf{u}(x, y, 0)$.

The reader is referred to Refs. [18,23] for a derivation of the plate equations and constitutive relations. When expansions for stresses are postulated to be independent of those for displacements and a mixed variational principle is employed, the resulting plate theory is called mixed HOSNDPT. However, for stresses derived from the expansions of displacements and Hooke's law, Batra et al. [23] called the resulting plate theory compatible HOSNDPT.

2.2. Weak formulation of the problem

Neglecting body forces, transient deformations of the plate are governed by

$$\begin{aligned} &\operatorname{div} \boldsymbol{\sigma} = \rho \ddot{\mathbf{u}}, && \text{in } \Omega \times (0,T), \\ &\boldsymbol{\sigma}\mathbf{n} = \bar{\mathbf{f}}, && \text{on } \Gamma_f \times \left[-\frac{h}{2}, \frac{h}{2}\right] \times (0,T), \\ &\mathbf{u} = \bar{\mathbf{u}}, && \text{on } \Gamma_u \times \left[-\frac{h}{2}, \frac{h}{2}\right] \times (0,T), \\ &\boldsymbol{\sigma}\mathbf{n} = \mathbf{q}^{\pm}, && \text{on } S^{\pm} \times (0,T), \\ &\mathbf{u}(x,y,z,0) = \mathbf{u}^0(x,y,z), && \text{in } \Omega, \\ &\dot{\mathbf{u}}(x,y,z,0) = \dot{\mathbf{u}}^0(x,y,z), && \text{in } \Omega. \end{aligned} \tag{9}$$

Here, ρ is the mass density, div the three-dimensional divergence operator, and $\mathbf{n}$ an outward unit normal to the surface. S^+ and S^- are the top and the bottom surfaces of the plate where surface tractions are prescribed, respectively, as $\mathbf{q}^+$ and $\mathbf{q}^-$. $\mathbf{q}^+$ and $\mathbf{q}^-$ need not be normal to S^+ and S^-, respectively; thus both normal and tangential tractions may be applied to the upper and the lower surfaces of the plate. Batra and Vidoli [18] have analyzed deformations of a plate whose upper and lower surfaces are subjected to tangential tractions. Γ_u and Γ_f are parts of the boundary ∂S of S. On $\Gamma_u \times [(-h/2), h/2]$ and $\Gamma_f \times [(-h/2), h/2]$ displacements and surface tractions are prescribed as $\bar{\mathbf{u}}$ and $\bar{\mathbf{f}}$, respectively. Eq. (9a) is the balance of linear momentum, Eqs. (9b)–(9d) are boundary conditions, and Eqs. (9e) and (9f) are initial conditions.

Let $\tilde{u}, \tilde{v}$ and $\tilde{w}$ be three linearly independent functions of $\mathbf{x}$ defined on Ω. Like u, v and w in Eq. (2), $\tilde{u}, \tilde{v}$ and $\tilde{w}$ are expanded in terms of Legendre polynomials $L_i(z)$. Multiplication of the three Eq. (9a) expressing the balance of linear momentum in x, y and z directions by $\tilde{u}, \tilde{v}$ and $\tilde{w}$, respectively, addition of the resulting three equations, the use of the divergence theorem and natural boundary conditions (9b) give

$$\int_{\Omega} \tilde{\boldsymbol{\varepsilon}}^{\mathrm{T}} \boldsymbol{\sigma}\, \mathrm{d}\Omega - \int_{\partial_u \Omega_m} \tilde{\mathbf{u}}^{\mathrm{T}} \boldsymbol{\sigma}\mathbf{n}\, \mathrm{d}\Gamma - \int_{\partial_f \Omega_m} \tilde{\mathbf{u}}^{\mathrm{T}} \bar{\mathbf{f}}\, \mathrm{d}\Gamma - \int_{S^+} \tilde{\mathbf{u}}^{\mathrm{T}} \mathbf{q}^{+} \mathrm{d}\Gamma - \int_{S^-} \tilde{\mathbf{u}}^{\mathrm{T}} \mathbf{q}^{-}\, \mathrm{d}\Gamma + \int_{\Omega} \rho \tilde{\mathbf{u}}^{\mathrm{T}} \ddot{\mathbf{u}}\, \mathrm{d}\Omega = 0. \tag{10}$$

Here, $\bar{\boldsymbol{\varepsilon}}$ is the six-dimensional strain vector derived from displacements $\tilde{\mathbf{u}} = (\tilde{u}, \tilde{v}, \tilde{w})$, and $\partial_u \Omega_m$ and $\partial_f \Omega_m$ are parts of the boundary $\partial \Omega_m$ of the mantle or the lateral surface of the plate where displacements and surface tractions are prescribed as $\bar{\mathbf{u}}$ and $\bar{\mathbf{f}}$, respectively; $\partial_u \Omega_m = \Gamma_u \times [(-h/2), h/2], \partial_f \Omega_m = \Gamma_f \times [(-h/2), h/2]$. Substitution from Eqs. (4), (6), and (9b)–(9d) into Eq. (10) and integration with respect to z from $-h/2$ to $h/2$ give

$$\sum_{i=0}^{K} \sum_{j=0}^{K} \left[\int_S \rho_{ij} \{\tilde{u}_i\}^{\mathrm{T}} \{\ddot{u}_j\} \mathrm{d}S + \int_S \{\tilde{\eta}_i\}^{\mathrm{T}} [D_{ij}] \{\eta_j\} \mathrm{d}S - \int_{\Gamma_u} \{\tilde{u}_i\}^{\mathrm{T}} [n] [D_{ij}] \{\eta_j\} \mathrm{d}\Gamma \right] = \sum_{i=0}^{K} \left[\int_{\Gamma_f} \{\tilde{u}\}_i^{\mathrm{T}} \{\bar{f}_i\} \mathrm{d}\Gamma + L_i\left(\pm \frac{h}{2}\right) \int_S \{\tilde{u}_i\}^{\mathrm{T}} \{q^{\pm}\} \mathrm{d}S \right], \tag{11}$$

where

$$\{\bar{f}_i\} = \int_{-h/2}^{h/2} L_i(z) \{\bar{f}\} \mathrm{d}z, \qquad \rho_{ij} = \int_{-h/2}^{h/2} \rho L_i(z) L_j(z) \mathrm{d}z, \qquad [D_{ij}] = \int_{-h/2}^{h/2} [D] L_i(z) L_j(z) \mathrm{d}z. \tag{12}$$

Square matrix $[\rho_{ij}]$ has $(K+1)$ rows and columns. The size of the matrix $[D_{ij}]$ is $6(K+1) \times 6(K+1)$. Since material properties are assumed to vary in the thickness direction only, ρ_{ij} and D_{ij} are independent of x and y. In the MLPG formulation, it is not necessary to require that $\{\tilde{u}_i\}$ vanish on Γ_u as is often done in the Galerkin formulation of the problem. Essential boundary conditions are imposed either by the penalty method or by the method of Lagrange multipliers or by static condensation in which the prescribed degrees of freedom are eliminated before solving the system of algebraic equations. For a plate made of a homogeneous material, Eqs. (12b) and (12c) simplify to

$$\rho_{ij} = \rho \delta_{ij}, \quad [D_{ij}] = [D] \delta_{ij}. \tag{13}$$

2.3. Semidiscrete formulation

Let M nodes be placed on the midsurface S of the plate, and $S_1, S_2, \ldots, S_M$ be smooth two-dimensional closed regions, not necessarily disjoint and of the same shape and size, enclosing nodes $1, 2, \ldots, M$, respectively. The union of $S_1, S_2, \ldots, S_M$ covers S. Let $\phi_1, \phi_2, \ldots, \phi_N$ and $\psi_1, \psi_2, \ldots, \psi_N$ be linearly independent functions defined on one of these regions, say S_α. For a Kth order plate theory there are $3(K+1)$ unknowns $u_0, v_0, w_0, u_1, v_1, w_1, \ldots, u_K, v_K, w_K$ at every point in S and hence in S_α. We write these as a $3(K+1)$ dimensional array $\{u\}$, and set

$$\{u(x, y, t)\} = \sum_{J=1}^{N} [\phi_J(x, y)] \{\delta_J(t)\}, \tag{14}$$

$$\{\tilde{u}(x, y)\} = \sum_{J=1}^{N} [\psi_J(x, y)] \{\tilde{\delta}_J\}, \tag{15}$$

where, for each value of J $\{\delta_J\}$ is a $3(K+1)$ dimensional array of fictitious nodal displacements and $\{\phi_J\}$ is a square matrix of $3(K+1)$ rows. Similar remarks apply to $\{\tilde{\delta}_J\}$ and $\{\psi_J\}$. Note that $\{\delta_J\}$ are functions of time t but $\{\tilde{\delta}_J\}$ are not functions of time. As will become clear from the discussion in Section 2.4, $\{\delta_J\}$ are not necessarily values of $\{u\}$ at node J since the basis functions $\{\phi_J\}$ do not have the Kronecker delta property. Substitution of Eqs. (14) and (15) into Eq. (5) gives

$$\{\eta\} = \sum_{J=1}^{N} [B_J] \{\delta_J\}, \qquad \{\tilde{\eta}\} = \sum_{J=1}^{N} [\tilde{B}_J] \{\tilde{\delta}_J\}, \tag{16}$$

where $\{\eta\}$ and $\{\tilde{\eta}\}$ are $6(K+1)$ dimensional arrays, and $[B]$ and $[\tilde{B}]$ are $6(K+1) \times 3(K+1)$ matrices. Elements of matrix $[B]$ involving functions ϕ_J and their partial derivatives with respect to x and y are listed in Refs. [21,22].

Writing Eq. (11) for $S = S_\alpha$, substituting for $\{\eta\}$, $\{\tilde{\eta}\}$, $\{u\}$ and $\{\tilde{u}\}$ from Eqs. (16), (14) and (15), requiring that the resulting equation hold for all choices of $\{\tilde{\delta}\}$, we arrive at the following system of coupled ordinary differential equations (ODEs):

$$[M_{IJ}] \{\ddot{\delta}_J\} + [K_{IJ}] \{\delta_J\} = \{F_I\}. \tag{17}$$

Here

$$[M_{IJ}] = \int_{S_\alpha} [\psi_I]^{\mathrm{T}} [\rho] [\phi_J] \mathrm{d}S, \tag{18}$$

$$[K_{IJ}] = \int_{S_\alpha} ([\tilde{B}_I]^{\mathrm{T}} [D] [B_J]) \mathrm{d}S - \int_{\Gamma_{\alpha u}} ([\psi_I]^{\mathrm{T}} [n] [D] [B_J]) \mathrm{d}\Gamma - \int_{\Gamma_{\alpha 0}} ([\psi_I]^{\mathrm{T}} [n] [D] [B_J]) \mathrm{d}\Gamma, \tag{19}$$

$$\{F_I\} = \int_{\Gamma_{\alpha f}} [\psi_I]^{\mathrm{T}} \{\bar{f}_i\} \mathrm{d}\Gamma + L_i(\pm h/2) \int_{S_\alpha} [\psi_I]^{\mathrm{T}} \{q^{\pm}\} \mathrm{d}S, \quad (20)$$

where $\Gamma_{\alpha 0} = \partial S_\alpha - \Gamma_{\alpha u} - \Gamma_{\alpha f}$, $\Gamma_{\alpha u} = \partial S_\alpha \cap \Gamma_u$ and $\Gamma_{\alpha f} = \partial S_\alpha \cap \Gamma_f$. The $(K+1)\times(K+1)$ matrix $[\rho]$ is expanded to the $3(K+1)\times 3(K+1)$ matrix in the usual way by multiplying each element of $[\rho]$ by a 3×3 identity matrix. Matrices $[K_{IJ}], [M_{IJ}]$ and $\{F_I\}$ are usually called the stiffness matrix, the mass matrix and the load vector, respectively. In the MLPG formulation, **M** and **K** need not be symmetric. Eq. (17) are derived for each S_α, $\alpha = 1, 2, \ldots, M$. There is no assembly of equations required in the MLPG method.

In order to derive initial conditions on $\{\delta_J\}$, we substitute from Eqs. (2) and (14) into Eq. (9e), multiply both sides of the resulting equation by $\{\tilde{u}\}^{\mathrm{T}}$, integrate it over S_α and exploit the fact that it must hold for all choices of $\{\tilde{\delta}_J\}$. The result is

$$\left[\int_{S_\alpha} \{\psi\}^{\mathrm{T}} \{\phi\} \mathrm{d}S\right] \{\delta(0)\} = \int_{S_\alpha} \{\psi\}^{\mathrm{T}} \{u(x,y,0)\} \mathrm{d}S. \quad (21)$$

A similar procedure is adopted to find $\{\dot{\delta}(0)\}$. For $\mathbf{u}^0 = \dot{\mathbf{u}}^0 = \mathbf{0}$, $\{\delta_J(0)\}$ and $\{\dot{\delta}_J(0)\}$ are null matrices. Essential boundary conditions are satisfied by using the method of static condensation to eliminate the prescribed degrees of freedom prior to solving the set of algebraic equations derived from the ODEs (17).

For a structure vibrating freely, $\{F_I\} = \{0\}$,

$$\{\delta_J(t)\} = \mathrm{e}^{\mathrm{i}\omega t} \{\bar{\delta}_J\}, \quad (22)$$

where $\{\bar{\delta}_J\}$ is the amplitude vector and ω is a natural frequency given by

$$\det[[K_{IJ}] - \omega^2 [M_{IJ}]] = 0. \quad (23)$$

Having found ω, the corresponding mode shape $\{\bar{\delta}_J\}$ is computed from

$$[K_{IJ}]\{\bar{\delta}_J\} = \omega^2 [M_{IJ}]\{\bar{\delta}_J\} \quad (24)$$

by suitably normalizing $\{\bar{\delta}_J\}$.

The basis functions $\{\phi_J\}$ in Eq. (14) are found by the moving least squares (MLS) method of Lancaster and Salkauskas [40].

2.4. Brief description of the MLS approximation

Let $f(x,y,t)$ be a scalar valued function defined on S_α; f can be identified with one of the displacements $u_0, v_0, w_0, u_1, v_1, w_1, \ldots, u_K, v_K, w_K$. The approximation $f^h(x,y,t)$ of f is assumed to be given by

$$f^h(x,y,t) = \sum_{j=1}^{m} p_j(x,y) a_j(x,y,t), \quad (25)$$

where

$$\mathbf{p}^{\mathrm{T}}(x,y) = \{1, x, y, x^2, xy, y^2, \ldots\} \quad (26)$$

is a complete monomial in x and y having m terms. For example, $\mathbf{p}^{\mathrm{T}} = \{1, x, y\}$ with $m = 3$ and $\mathbf{p}^{\mathrm{T}} = \{1, x, y, x^2, xy, y^2\}$ with $m = 6$ are, respectively, complete monomials of degree 1 and 2. The m unknown coefficients $a_j(x,y,t)$ are determined by minimizing $J(\mathbf{x},t)$ defined below by Eq. (27) with respect to $a_1(x,y,t), a_2(x,y,t), \ldots, a_m(x,y,t)$:

$$J(\mathbf{x},t) = \sum_{i=1}^{n} W(\mathbf{x}-\mathbf{x}_i)[\mathbf{p}^{\mathrm{T}}(\mathbf{x}_i)\mathbf{a}(\mathbf{x},t) - \hat{f}_i(t)]^2. \quad (27)$$

Here, $\hat{f}_i(t)$ is the fictitious value at time t of the function f at the point $\mathbf{x}_i = (x_i, y_i)$, and n is the number of points in the vicinity of $\mathbf{x}$ for which the weight function $W(\mathbf{x}-\mathbf{x}_i) > 0$. W is a non-negative function of $\mathbf{x}$ and vanishes for $|\mathbf{x} - \mathbf{x}_i| \geq r_w$, where r_w is the radius of the compact support of W. When a quadrature point used to numerically evaluate integrals appearing in Eqs. (18)–(20) is located at $\mathbf{x}$, then the n-points in Eq. (27) can be taken from the M nodes placed on S. We take

$$W(\mathbf{x}-\mathbf{x}_i) = \begin{cases} 1 - 6\left(\dfrac{d_i}{r_w}\right)^2 + 8\left(\dfrac{d_i}{r_w}\right)^3 - 3\left(\dfrac{d_i}{r_w}\right)^4, & 0 \leq d_i \leq r_w, \\ 0, & d_i \geq r_w, \end{cases} \quad (28)$$

where $d_i = |\mathbf{x} - \mathbf{x}_i|$ is the distance between points $\mathbf{x}$ and $\mathbf{x}_i$, and r_w is the radius of the circle outside of which W vanishes.

Setting $\partial J/\partial a_l = 0$, for $l = 1, 2, \ldots, n$, we obtain the following system of linear algebraic equations for the determination of $a_1(\mathbf{x},t), a_2(\mathbf{x},t), \ldots, a_n(\mathbf{x},t)$:

$$\mathbf{A}(\mathbf{x})\mathbf{a}(\mathbf{x},t) = \mathbf{B}(\mathbf{x})\hat{\mathbf{f}}(t), \quad (29)$$

where

$$\begin{aligned} \mathbf{A}(\mathbf{x}) &= \sum_{i=1}^{n} W(\mathbf{x}-\mathbf{x}_i)\mathbf{p}^{\mathrm{T}}(\mathbf{x}_i)\mathbf{p}(\mathbf{x}_i), \\ \mathbf{B}(\mathbf{x}) &= [W(\mathbf{x}-\mathbf{x}_1)\mathbf{p}(\mathbf{x}_1), W(\mathbf{x}-\mathbf{x}_2)\mathbf{p}(\mathbf{x}_2), \ldots, \\ &\quad W(\mathbf{x}-\mathbf{x}_n)\mathbf{p}(\mathbf{x}_n)]. \end{aligned} \quad (30)$$

Substitution for $\mathbf{a}(\mathbf{x},t)$ from Eq. (29) into Eq. (25) yields

$$f^h(\mathbf{x},t) = \sum_{j=1}^{m} \phi_j(\mathbf{x}) \hat{f}_j(t), \quad (31)$$

where

$$\phi_k(\mathbf{x}) = \sum_{j=1}^{m} p_j(\mathbf{x})[\mathbf{A}^{-1}(\mathbf{x})\mathbf{B}(\mathbf{x})]_{jk} \quad (32)$$

are the basis functions of the MLS approximation. Note that $\phi_k(x_j) \neq \delta_{kj}$; thus $\hat{f}_i(t) \neq f^h(x_i, y_i, t)$. For the matrix **A** to be invertible, $n \geq m$. For $m = 3$ or 6, Chati and Mukherjee [41] have suggested that $15 \leq n \leq 30$ for two-dimensional elastostatic problems.

For a two-dimensional elastodynamic problem, Batra and Ching [34] used Gauss weight functions, $m = 6$, and $r_w = 3.5$ times the distance between the point $\mathbf{x}_i$ and the third node nearest to the node at $\mathbf{x}_i$. Here, we take

$$r_w = ch_i, \tag{33}$$

where h_i is the distance from the node at $\mathbf{x}_i$ to the node nearest to it and c is a scaling parameter.

2.5. Numerical integration of ODEs

The Newmark family of methods [42] is used to numerically integrate the system (17) of coupled second-order ODEs. The recursive relation among displacements, velocities and accelerations at times t_n and $t_{n+1} = t_n + \Delta t$ are

$$\begin{aligned}\boldsymbol{\delta}^{n+1} &= \boldsymbol{\delta}^n + \Delta t\dot{\boldsymbol{\delta}}^n + \frac{\Delta t^2}{2}[(1-2\beta)\ddot{\boldsymbol{\delta}}^n + 2\beta\ddot{\boldsymbol{\delta}}^{n+1}],\\ \dot{\boldsymbol{\delta}}^{n+1} &= \dot{\boldsymbol{\delta}}^n + \Delta t[(1-\gamma)\ddot{\boldsymbol{\delta}}^n + \gamma\ddot{\boldsymbol{\delta}}^{n+1}],\end{aligned} \tag{34}$$

where $\boldsymbol{\delta}^n \simeq \boldsymbol{\delta}(t_n)$, etc. and β and γ are constants. We set $\gamma = 0.5$ and $\beta = 0.25$; then the Newmark method is equivalent to the constant average acceleration method. It is non-dissipative, second-order accurate and unconditionally stable.

Writing Eq. (17) at time t_{n+1}, and substituting from Eq. (34) give the following system of algebraic equations

$$\hat{\mathbf{K}}^{n+1}\boldsymbol{\delta}^{n+1} = \hat{\mathbf{F}}^{n+1}, \tag{35}$$

where

$$\begin{aligned}\hat{\mathbf{K}}^{n+1} &= \mathbf{K}^{n+1} + \frac{4}{\Delta t^2}\mathbf{M}^{n+1},\\ \hat{\mathbf{F}}^{n+1} &= \mathbf{F}^{n+1} + \mathbf{M}^{n+1}\left(\frac{4}{\Delta t^2}\hat{\boldsymbol{\delta}}^n + \frac{4}{\Delta t}\dot{\hat{\boldsymbol{\delta}}}^n + \ddot{\hat{\boldsymbol{\delta}}}^n\right).\end{aligned} \tag{36}$$

Having computed $\boldsymbol{\delta}^{n+1}$ from Eq. (35), $\ddot{\boldsymbol{\delta}}^{n+1}$ and $\dot{\boldsymbol{\delta}}^{n+1}$ are obtained from

$$\begin{aligned}\ddot{\boldsymbol{\delta}}^{n+1} &= \frac{4}{\Delta t^2}(\boldsymbol{\delta}^{n+1} - \boldsymbol{\delta}^n) - \frac{4}{\Delta t}\dot{\boldsymbol{\delta}}^n - \ddot{\boldsymbol{\delta}}^n,\\ \dot{\boldsymbol{\delta}}^{n+1} &= \dot{\boldsymbol{\delta}}^n + \frac{\Delta t}{2}(\ddot{\boldsymbol{\delta}}^n + \ddot{\boldsymbol{\delta}}^{n+1}).\end{aligned} \tag{37}$$

2.6. Satisfaction of essential boundary conditions

Eq. (35) is separated into two groups: $\boldsymbol{\delta}_p^{n+1}$ for nodes where displacements are prescribed, and $\boldsymbol{\delta}_f^{n+1}$ for the remaining nodes. Using Eq. (14), equations for $\boldsymbol{\delta}_p^{n+1}$ are replaced by

$$\bar{\mathbf{u}}(x_i, y_i, t_{n+1}) = \sum_{J=1}^{n} \phi_J(x_i, y_i)\boldsymbol{\delta}_J^{n+1}, \qquad i = 1, 2, \ldots, N_p, \tag{38}$$

where N_p equals the number of nodes where displacement $\mathbf{u}$ is prescribed as $\bar{\mathbf{u}}$.

2.7. Estimation of effective elastic constants

Methods that have been proposed to find the effective moduli of a composite of two constituents include the rule of mixture, the three-phase model of Fröhlich and Sack [43], the self-consistent scheme [44], the Mori–Tanaka technique [24], the mean field approach [45], and the representative volume element. Vel and Batra [13,14,46] used the Mori–Tanaka and the self-consistent methods to find an analytical solution for static and dynamic deformations of a simply supported FG plate. They found that the two homogenization techniques give different results. Even though the rule of mixtures is easiest to use, it gives very approximate values of the effective elastic moduli and does not account for the interaction among adjacent inclusions. The Mori–Tanaka method accounts for these interactions and has rather simple relations to find the bulk modulus K_e and the shear modulus μ_e of the equivalent homogenized medium. We adopt it here and find the effective mass density from the rule of mixtures, and K_e and μ_e from

$$\begin{aligned}\frac{K_e - K_1}{K_2 - K_1} &= \frac{V_2}{1 + (1-V_2)(3(K_2-K_1)/(3K_1+4\mu_1))},\\ \frac{\mu_e - \mu_1}{\mu_2 - \mu_1} &= \\ &\frac{V_2}{1+(1-V_2)(\mu_2-\mu_1)/(\mu_1+\mu_1(9K_1+8\mu_1)/6(K_1+2\mu_1))}.\end{aligned} \tag{39}$$

Here, K_1 and μ_1 are, respectively, the bulk modulus and the shear modulus of constituent 1 with volume fraction V_1, and K_2, μ_2 and V_2 are the corresponding quantities for constituent 2. Note that $V_2 = 1 - V_1$. It has been tacitly assumed here that each of the two constituents is isotropic and the macroscopic response of the composite is also isotropic. A fiber reinforced plate is usually modeled as orthotropic, and the material moduli are determined experimentally. Closed form relations like Eq. (39) are not readily available since elastic constants will likely also depend upon the cure cycle. If elastic constants as a function of the volume fraction are known, then the present analysis can be adopted for functionally graded orthotropic plates. One way to obtain FG anisotropic plates is to continuously vary the fiber orientation through the plate thickness [57].

3. Results and discussion

Boundary conditions imposed at a simply supported (S), a clamped (C) and a free (F) edge are:

$$\begin{aligned}&S: \sigma_{xx} = 0,\ v = w = 0,\ \text{on } x = 0, a;\\ &\sigma_{yy} = 0,\ u = w = 0,\ \text{on } y = 0, b;\\ &C: u = v = w = 0,\ \text{on } x = 0, a;\ y = 0, b;\\ &F: \sigma_{xx} = \sigma_{yx} = \sigma_{zx} = 0,\ \text{on } x = 0, a;\\ &\sigma_{yy} = \sigma_{xy} = \sigma_{zy} = 0,\ \text{on } y = 0, b\end{aligned} \tag{40}$$

Whereas boundary conditions (40c) at a free edge can be easily realized in a laboratory, Eqs. (40a) and (40b) for simply supported and clamped edges cannot be well satisfied in a laboratory setting. One could invoke St Venant's principle and say that the computed solution is valid at points away from the edges. In a laboratory, plates are either supported on sharp knife edges or rollers or are clamped in a vice. In practice, plate edges are generally fixed to supports by screws or bolts or are welded. If the material of the supports is assumed to be rigid, then welded edges satisfy boundary conditions (40b) stipulated for clamped edges. Boundary conditions (40a) for a simply supported edge have been employed by Vlasov [47], Srinivas et al. [48] and Pagano [49] to find analytical solutions of three-dimensional elasticity equations. Several researchers have subsequently adopted them. Boundary conditions used by Batra and Geng [50,51] closely simulate those applicable to plates supported on rollers.

Henceforth, we will use S to denote a simply supported edge rather than the midsurface of the plate.

A computer code has been developed to analyze static deformations, and free and forced vibrations of a FG thick plate. It has been validated by comparing computed results for homogeneous plates with the analytical solutions of the corresponding problems [13,14,46]. For inhomogeneous plates, as shown below, results for static deformations and the computed natural frequencies agree very well with the corresponding analytical values.

Previous studies of homogeneous thick plates and numerical experiments with FG thick plates having aspect ratio (length/thickness) 5 with the MLPG method have given that the following values of different variables in the MLPG technique yield very good results:

$$K = 5,\ \ m = 15,\ \ c = 15,\ \ N = 13 \times 13 = 169,$$
$$N_Q = 9 \times 9 = 81.$$

That is, a fifth-order plate theory is adequate, complete fourth-order monomials should be considered in Eq. (25) to generate the MLS basis functions, the radius of the support of the weight function W in Eq. (28) should equal 15 times the distance from the node at $\mathbf{x}_i$ to the node closest to it, and 81 integration points, N_Q, ought to be used to evaluate integrals appearing in Eqs. (18)–(20). S_α equals a circular region with center at $\mathbf{x}_\alpha$ and radius equal to the distance from the node at $\mathbf{x}_\alpha$ to the nearest node. Functions $\{\phi_J\}$ in Eq. (14) are the MLS basis functions. For the node at $\mathbf{x}_\alpha$, $\psi_J(x, y)$ in Eq. (15) equals $W(\mathbf{x} - \mathbf{x}_\alpha)$ with support equal to S_α. Thus integrations in Eqs. (18)–(20) are to be performed over a circular region. For evaluating these integrals numerically, a circle is mapped onto a square of size 2×2 and Gaussian integration points with the corresponding weights are employed as in the FEM. Thirteen equally spaced nodes, in the x and y-directions, as shown in Fig. 2, are sufficient. Thus for a free plate the total number of degrees of freedom equals $3 \times 6 \times 169 = 3042$.

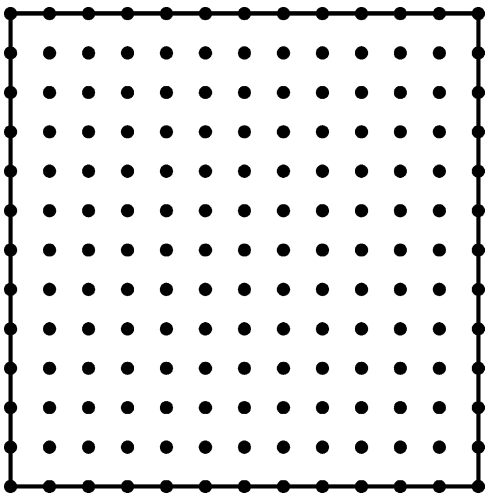

Fig. 2. Locations of 169 uniformly distributed nodes on the midsurface of the plate.

The consisent mass matrix is used to compute solutions of dynamic problems. Note that no background mesh is used to evaluate integrals in Eqs. (18)–(20). As will be evident from the results presented below, the above listed values of K, m, c, N and N_Q give results for FG plates with different volume fractions of constituents that are close to the analytical solution of the corresponding problems. Convergence studies for different values of K, m, c, N and N_Q were conducted in Refs. [21,22]; those results should be valid for the present problem also since Eq. (17) is similar to those for a homogeneous plate.

We compute results for a FG plate comprised of either aluminum and zirconia or aluminum and a ceramic (SiC) mainly because analytical results [13,14,46] for a plate made of these materials are available for comparison. Material properties of the aluminum (Al), zirconia (ZrO_2) and ceramic (SiC) are

$$\text{Al} : E_m = 70\ \text{GPa},\ \ \nu_m = 0.3,\ \ \rho_m = 2702\ \text{kg/m}^3,$$
$$\text{ZrO}_2 : E_z = 200\ \text{GPa},\ \ \nu_z = 0.3,\ \ \rho_z = 5700\ \text{kg/m}^3, \quad (41)$$
$$\text{SiC} : E_c = 427\ \text{GPa},\ \ \nu_c = 0.17,\ \ \rho_c = 3100\ \text{kg/m}^3.$$

Here, E is the Young's modulus and ν the Poisson ratio; these are related to K and μ by $K = E/3(1 - 2\nu)$ and $\mu = E/2(1 + \nu)$. We assume that the volume fraction of the ceramic phase is given by

$$V_c = V_c^- + (V_c^+ - V_c^-)\left(\frac{1}{2} + \frac{z}{h}\right)^p, \quad (42)$$

where V_c^+ and V_c^- are, respectively, the volume fractions of the ceramic phase on the top and the bottom surfaces of the plate, and the parameter p dictates the volume fraction profile through the thickness. For example, for an aluminum/zirconia FG plate, $p = 0$ corresponds to a homogeneous plate with a uniform distribution, V_c^+, of

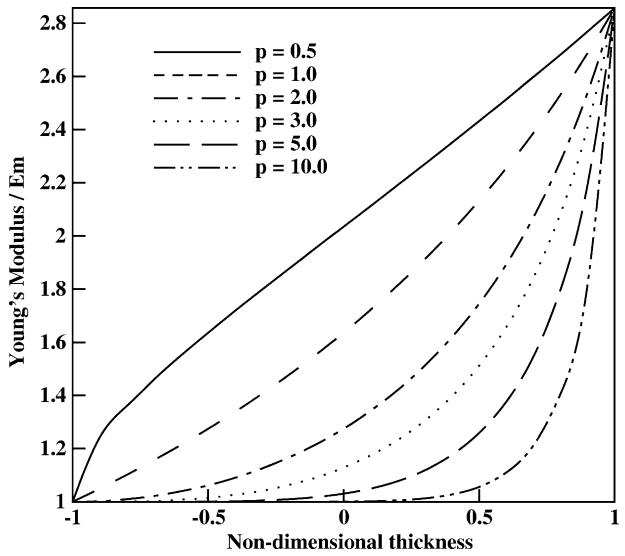

Fig. 3. Variation of Young's modulus with the non-dimensional thickness for different values of the exponent p in Eq. (42).

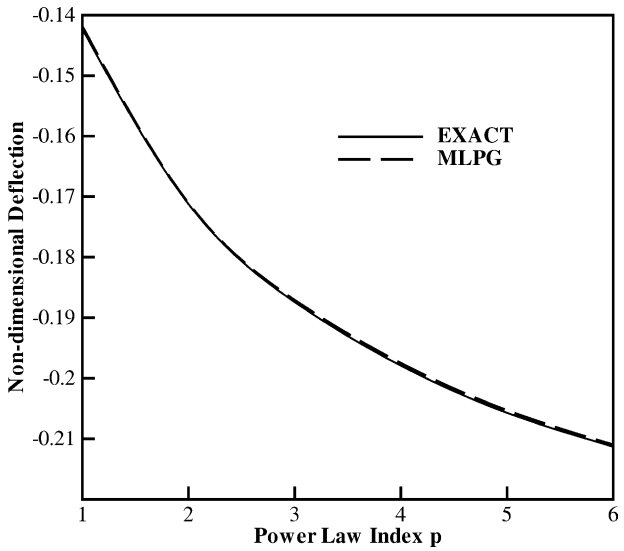

Fig. 4. Comparison of the presently computed centroidal deflection of an Al/SiC FG plate with the analytical solution of Vel and Batra [46].

zirconia, and $p = \infty$ to a homogeneous plate with a uniform distribution, V_c^-, of zirconia. Through-the-thickness variations of E for different values of p are exhibited in Fig. 3. For $0 \le V_c \le 1$, the Poisson ratio was found to vary between 0.294 and 0.3; it has been taken as 0.3 throughout the plate. For an Al/SiC plate, E and ν will be functions of z.

In the Tables and Figures to follow, vertical or transverse displacement w, longitudinal or axial stress σ_{xx}, thickness coordinate z, and frequency ω have been non-dimensionalized as follows:

$$\bar{w} = \frac{100E_m h^3}{12a^4(1-\nu_m^2)q_0}w, \qquad \bar{\sigma}_{xx} = \frac{h^2}{a^2 q_0}\sigma_{xx}, \qquad \bar{z} = \frac{2z}{h}, \qquad \bar{\omega} = \omega h\sqrt{\rho_m/E_m}. \tag{43}$$

Here, a is the length of a square plate, q_0 is either the amplitude or the intensity of the uniformly distributed load applied on the top surface of the plate, and an overbar signifies a non-dimensional quantity.

3.1. Static problems

3.1.1. Comparison of computed results with the analytical solution

Figs. 4 and 5 compare, respectively, the numerical and the analytical solutions for the transverse deflection of the plate centroid and the axial stress at the centroid of the top surface of the simply supported Al/SiC square FG plate. The top surface of the plate is loaded by a normal pressure given by $q_0 \sin \pi x/a \sin \pi y/a$ and the bottom surface of the plate is traction free. Note that any traction applied on the top surface can be represented as a Fourier series and the solution obtained by the method of superposition. It thus suffices to consider the pressure given by $q_0 \sin \times \pi x/a \sin(\pi y/b)$. We have set $V_c^- = 0$, $V_c^+ = 1.0$ and $h/a = 0.2$. The analytical solution is due to Vel and Batra [46]. It is clear that the numerical solution of the problem with the compatible HOSNDPT and the MLPG method agrees very well with the analytical solution. A comparison of results given in Fig. 3 of Vel and Batra [46] with those plotted in our Figs. 4 and 5 reveals that the compatible fifth-order HOSNDPT gives results much closer to the analytical solution than those obtained from the third-order shear deformation theory (TSDT); results with the TSDT are given in Ref. [46]. Since the axial stresses at the centroid of the top surface of the plate computed from the solutions of

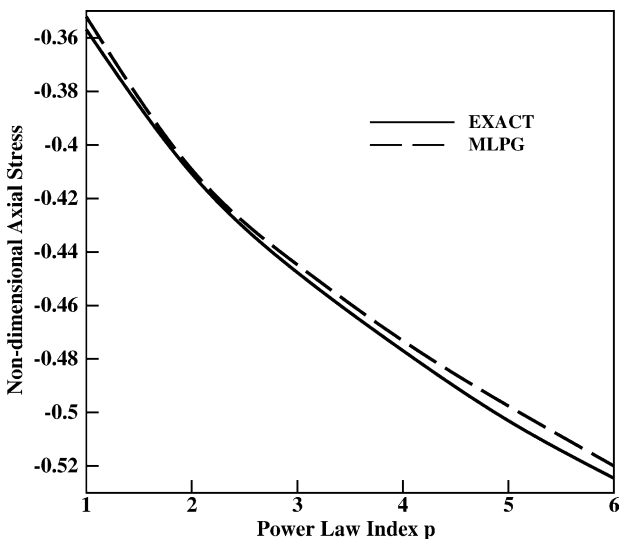

Fig. 5. Comparison of the presently computed axial stress at the centroid of the top surface of an Al/SiC FG plate with the analytical solution of Vel and Batra [46].

the classical plate theory, the first-order shear deformation theory and the TSDT were essentially the same (Fig. 3e of Ref. [46]) it appears that the consideration of normal deformations has given axial stress significantly closer to the analytical value.

3.1.2. Results for a uniformly distributed pressure on the top surface of a FG plate

For an Al/SiC simply supported FG plate, Figs. 6 and 7 depict, respectively, the through-the-thickness variation, at points on the centroidal axis, of the transverse displacement $\bar{w}$ and of the axial stress $\bar{\sigma}_{xx}$ for different values of the exponent p in Eq. (42). It is clear that even for a homogeneous plate the transverse displacement is not symmetrical about the midsurface; note that the applied load is not symmetrical about the plate's midsurface. Analytical solution of the problem also exhibits this asymmetry [46]. From the plot of the through-the-thickness variation of the axial stress shown in Fig. 7, one can conclude that the maximum tensile stress at points on the bottom surface of a ceramic plate is reduced by adding aluminum to the ceramic and the magnitude of the compressive stress at points on the top surface is increased. The compressive strength of a ceramic is considerably larger than its tensile strength. For $p = 0.5, 1.0$ and 2.0, the stress distributions through the thickness of the plate are very close to each other and the transverse deflections are qualitatively similar. Transverse deflections decrease with an increase in the volume fraction of the ceramic in the plate since Young's modulus for the ceramic is nearly three times that of aluminum. The effect of varying the volume fraction of the ceramic at the top surface of the FG plate on the through-the-thickness variation at points on the centroidal axis of the transverse displacement $\bar{w}$ and the axial stress $\bar{\sigma}_{xx}$ is exhibited in Figs. 8 and 9, respectively. Whereas, through-the-thickness variation of the axial stress is not influenced that much by the value of V_c^+, the deflection varies noticeably with V_c^+.

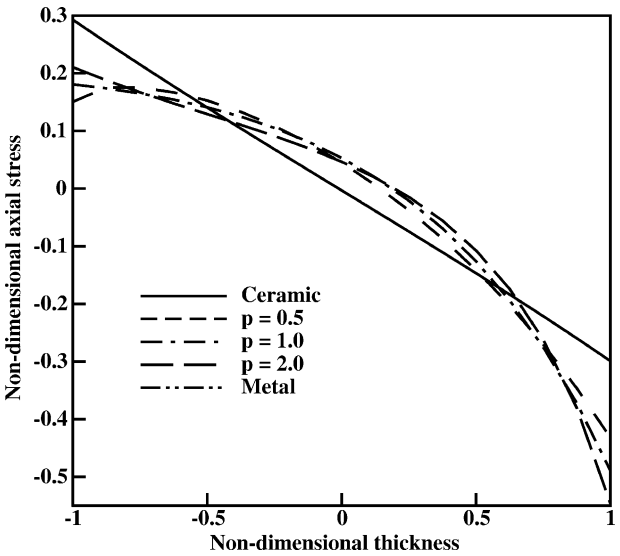

Fig. 7. For different values of the exponent p, non-dimensional axial stress at points on the centroidal axis in the simply-supported square FG plate with $a/h = 5$ under uniform load applied on the top surface of the plate.

3.2. Free vibrations

We compare our results for the natural frequencies of a simply supported Al/ZrO_2 FG plate with those of Vel and Batra [14] who solved the problem analytically.

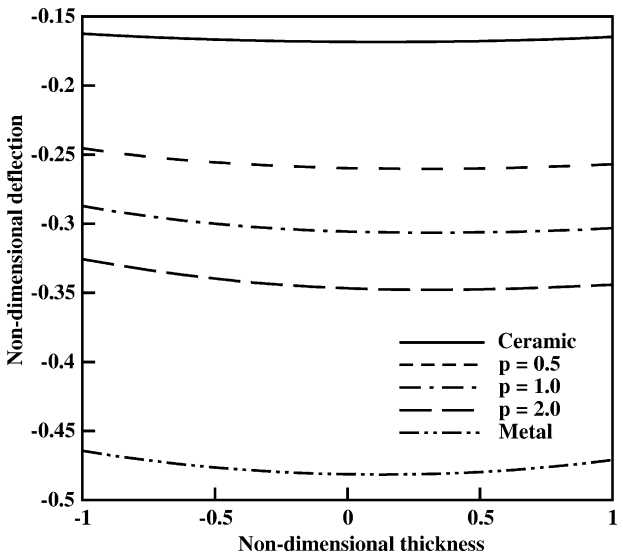

Fig. 6. For different values of the exponent p, through-the-thickness variation at points on the centroidal axis of the non-dimensional deflection of the simply-supported square FG plate with $a/h = 5$ under uniform load applied on the top surface of the plate.

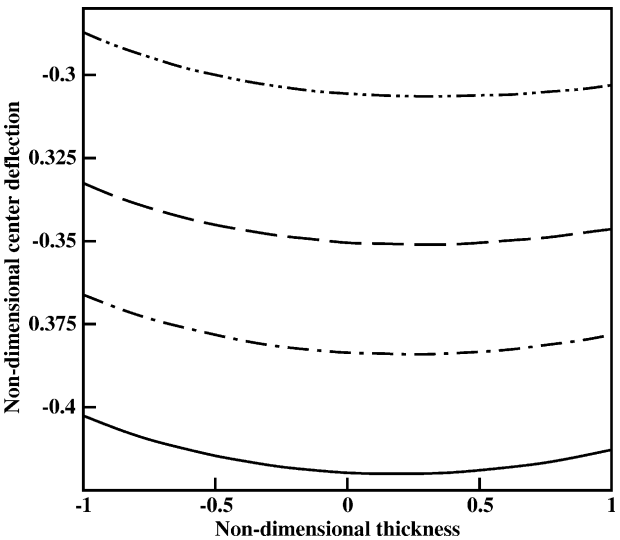

Fig. 8. For different values of V_c^+, non-dimensional deflection of the simply-supported square FG plate with $a/h = 5$ under uniform normal load applied on the top surface of the plate. — $V_c^+ = 0.3$, - ·- ·- $V_c^+ = 0.5$, - - - $V_c^+ = 0.7$, - ···- ··· $V_c^+ = 1.0$.

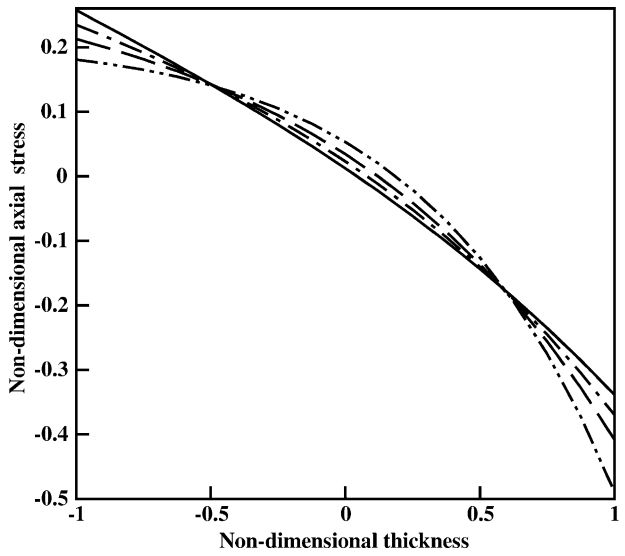

Fig. 9. For different values of V_c^+, through-the-thickness variation of the non-dimensional axial stress at points on the centroidal axis in a simply-supported square FG plate with $a/h = 5$ under uniform normal load applied on the top surface of the plate. — $V_c^+ = 0.3$, - ·- ·- $V_c^+ = 0.5$, - - - $V_c^+ = 0.7$, - ··- ··- $V_c^+ = 1.0$.

They assumed displacements of the form

$$\begin{Bmatrix} u(x,y,z,t) \\ v(x,y,z,t) \\ w(x,y,z,t) \end{Bmatrix} = \sum_{m,n=1}^{\infty} e^{i\omega_{mn}t} \begin{Bmatrix} U_{mn}(z)\cos\dfrac{m\pi x}{a}\sin\dfrac{n\pi y}{b} \\ V_{mn}(z)\sin\dfrac{m\pi x}{a}\cos\dfrac{n\pi y}{b} \\ W_{mn}(z)\sin\dfrac{m\pi x}{a}\sin\dfrac{n\pi y}{b} \end{Bmatrix}. \tag{44}$$

Batra and Aimmanee [52] have shown that the lower limit in the summation in Eq. (44) should be 0 in order not to miss any of the in-plane pure distortional modes of vibration which can occur in a FG plate only when μ/ρ is independent of z. Whereas the present method can rank frequencies from the lowest to the highest, in Vel and Batra's exact solution [14] they are computed by assigning different values to m and n. Presently computed results for different values of V_c^+, V_c^- and p are compared with those of Vel and Batra [14] in Tables 1–3, and the first 10 natural frequencies of a simply supported square FG plate are listed in Table 4.

Table 1
Comparison of thickness mode natural frequencies of a simply supported square Al/ZrO_2 FG thick plate with $V_c^- = 0$, $V_c^+ = 1$, $p = 1$, and $m = n = 1$ in Eq. (44)

Thickness mode	$h/a = 0.05$		$h/a = 0.10$		$h/a = 0.2$	
	Present	Exact	Present	Exact	Present	Exact
1	0.0149	0.0153	0.0584	0.0596	0.2152	0.2192
2	0.1457	0.1456	0.2913	0.2912	0.5820	0.5823
3	0.2448	0.2454	0.4872	0.4901	0.9687	0.9752
4	2.0334	2.0598	2.0788	2.0750	2.1696	2.1346

Table 2
Comparison of thickness mode natural frequencies of a simply supported square Al/ZrO_2 FG thick plate with $m = n = 1$ in Eq. (44), $V_c^- = 0$, $V_c^+ = 1$ and different values of p

Thickness mode	$p = 2$		$p = 3$		$p = 5$	
	Present	Exact	Present	Exact	Present	Exact
1	0.2153	0.2197	0.2172	0.2211	0.2194	0.2225
2	0.5709	0.5711	0.5659	0.5660	0.5612	0.5610
3	0.9494	0.9564	0.9414	0.9478	0.9346	0.9398
4	2.0154	2.0150	1.9586	1.9530	1.9204	1.9075

The presently computed natural frequency of the fourth thickness mode corresponding to $m = n = 1$ and for $a/h = 20$ listed in Table 1 differs from the exact value by less than 1.3%; the difference is less for the lower order thickness modes. For $a/h = 5$, the difference between the computed and the analytical frequencies of the fourth thickness mode with $m = n = 1$ is 1.64%. Results presented in Table 3 show that the frequencies of thickness modes associated with the first flexural mode are virtually unaffected by the values of V_c^+. Since the plate is square, therefore the second and the third lowest frequencies are identical; the same is true for the fourth and the fifth lowest frequencies. The second and third frequencies correspond to $m = 2$, $n = 1$ and $m = 1$, $n = 2$. Results given in Table 4 reveal that for $V_c^- = 0$ and $V_c^+ = 1$, natural frequencies of the pure ceramic and the pure metal plate are the upper and the lower bounds of the frequencies of an FG plate. The value of p, i.e. the precise through-the-thickness distribution of the ceramic phase has a minute effect on the natural frequencies of a FG plate. Also, for fixed values of V_c^-, p and a/h, the first 10 frequencies are not affected much by the value of V_c^+. However, the aspect ratio a/h of the plate has a noticeable influence on the first 10 natural frequencies.

3.3. Forced response

A time harmonic uniformly distributed normal pressure of $10 \sin 5000t$ is applied for $0 \le t \le 5$ ms to the top surface of a simply supported square Al/ZrO_2 FG plate with $a/h = 10$ and then suddenly removed. Fig. 10 depicts the time history of the centroidal deflection for the first 5 ms. The time period 1.25 ms of the centroidal deflection equals

Table 3
Comparison of thickness mode natural frequencies of a simply supported square Al/ZrO_2 FG thick plate with $m = n = 1$ in Eq. (44), $V_c^- = 0$, $p = 1$, $h/a = 0.2$ and different values of V_c^+

Thickness mode	$V_c^+ = 0.3$		$V_c^+ = 0.5$		$V_c^+ = 0.7$	
	Present	Exact	Present	Exact	Present	Exact
1	0.2109	0.2112	0.2112	0.2120	0.2122	0.2139
2	0.5509	0.5505	0.5550	0.5547	0.5627	0.5626
3	0.9224	0.9228	0.9278	0.9292	0.9393	0.9420
4	2.0893	2.0263	2.0847	2.0446	2.0192	2.0736

Table 4
First 10 natural frequencies of a simply supported square thick Al/ZrO_2 FG plate

	$V_c^- = 0$, $V_c^+ = 1$, $h/a = 0.2$					$V_c^- = 0$, $p = 1.0$, $h/a = 0.2$			$V_c^- = 0$, $V_c^+ = 1$, $p = 1.0$	
	Ceramic	$p = 1.0$	$p = 2.0$	$p = 5.0$	Metal	$V_c^+ = 0.3$	$V_c^+ = 0.5$	$V_c^+ = 0.7$	$h/a = 0.05$	$h/a = 0.1$
1	0.2469	0.2152	0.2153	0.2194	0.2122	0.2109	0.2112	0.2122	0.0149	0.0584
2	0.4535	0.4114	0.4034	0.3964	0.3897	0.3891	0.3920	0.3975	0.0377	0.1410
3	0.4535	0.4114	0.4034	0.3964	0.3897	0.3891	0.3920	0.3975	0.0377	0.1410
4	0.5441	0.4761	0.4720	0.4760	0.4675	0.4650	0.4659	0.4686	0.0593	0.2058
5	0.5441	0.4761	0.4720	0.4760	0.4675	0.4650	0.4659	0.4686	0.0747	0.2058
6	0.6418	0.5820	0.5709	0.5611	0.5517	0.5509	0.5550	0.5627	0.0747	0.2164
7	0.7881	0.6914	0.6817	0.6832	0.6772	0.6737	0.6753	0.6797	0.0769	0.2646
8	0.9076	0.8192	0.8056	0.7928	0.7615	0.7788	0.7844	0.7952	0.0912	0.2677
9	0.9326	0.8217	0.8105	0.8053	0.7799	0.7973	0.7993	0.8047	0.0913	0.2913
10	0.9354	0.8242	0.9022	0.8099	0.8013	0.8020	0.8040	0.8096	0.1029	0.3264

$2\pi/\omega = 1.257$ ms of the applied load for each one of the five values of p considered. The amplitude of the centroidal deflection of the FG plate is bounded by that of the pure ceramic and the pure metallic plates. The numerical integration scheme introduces a small damping even though the Newmark method is non-dissipative for $\gamma = 1/2$ and $\beta = 1/4$. The time history of the axial stress at the centroid of the top surface of the plate is plotted in Fig. 11. Figs. 12 and 13 show results similar to those plotted in Figs. 10 and 11 except that a uniformly distributed pressure equal to 10 is applied on the top surface of the plate for $0 \le t \le 2.5$ ms and then suddenly removed. It is clear that the time period of the oscillations of the ceramic plate is less than that of the metallic plate. The time period of the metallic plate equals about 0.4 ms. As long as the pressure load acts on the plate, the plate centroid does not move above its horizontal undeformed position. Upon removal of the load, the plate oscillates about the horizontal equilibrium position.

4. Conclusions

The static and the dynamic response of a simply supported thick square functionally graded (FG) plate has been analyzed by using a compatible higher order shear and normal deformable plate theory (HOSNDPT) and a meshless local Petrov–Galerkin (MLPG) method. In the MLPG method, no background mesh is required to evaluate integrals appearing in the weak formulation of the problem. Effective material moduli have been determined by using

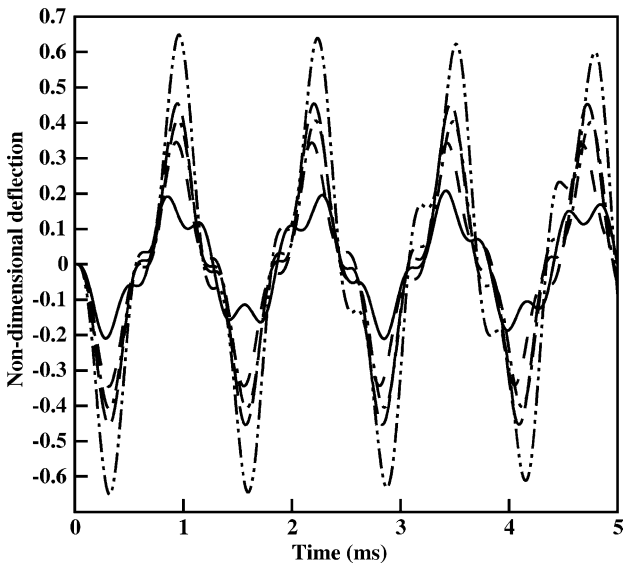

Fig. 10. Time history of the non-dimensional centroidal deflection of a simply supported square FG plate with the top surface loaded by a uniformly distributed pressure load of 10 sin 5000t for $0 \le t \le 5$ ms. — ceramic, - - - $p = 0.5$, - ·- ·- $p = 10$, – – – $p = 20$, - ···- ···- metal.

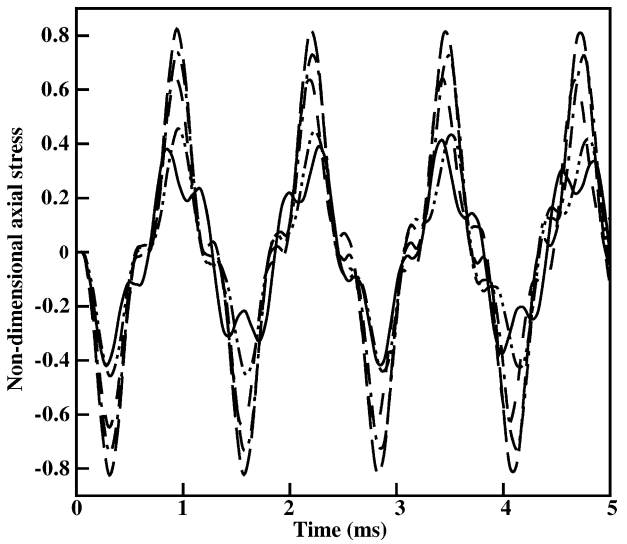

Fig. 11. Time history of the non-dimensional axial stress at the centroid of the top surface of a simply supported square FG plate loaded by a uniformly distributed pressure load of 10 sin 5000 t for $0 \le t \le 5$ ms. — ceramic, - - - $p = 0.5$, - ·- ·- $p = 10$, – – – $p = 20$, - ···- ···- metal.

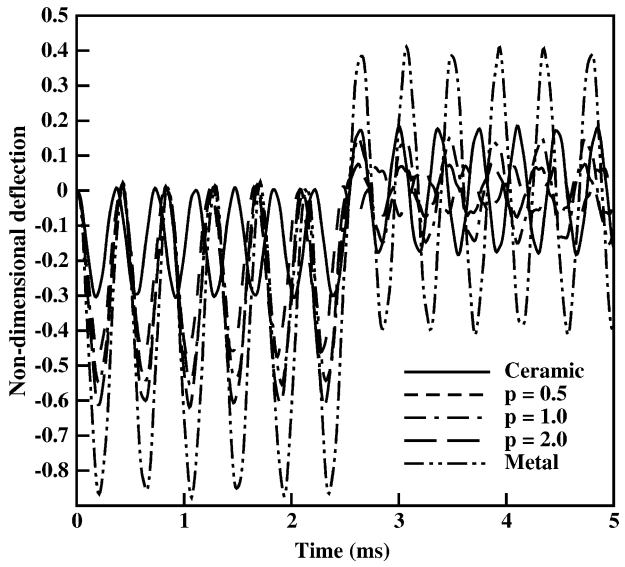

Fig. 12. Time-history of the non-dimensional centroidal deflection of a simply supported square FG plate with the top surface loaded by a uniformly distributed pressure of 10 for $0 \leq t \leq 2.5$ ms.

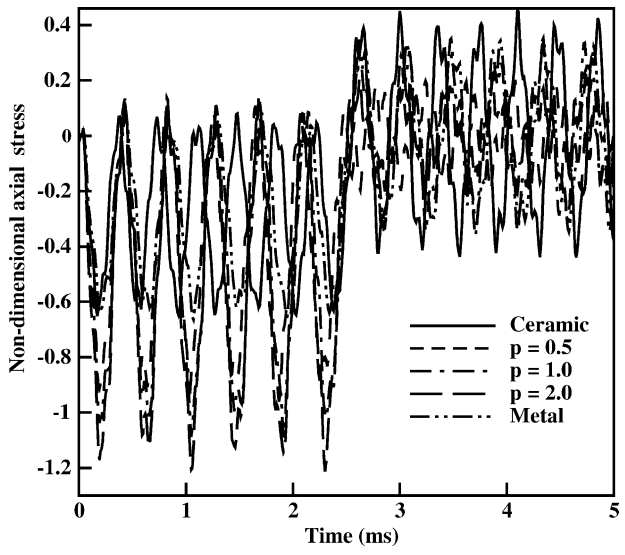

Fig. 13. Time-history of the non-dimensional axial stress at the centroid of the top surface of a simply supported square FG plate with the top surface loaded by a uniformly distributed pressure of 10 for $0 \leq t \leq 2.5$ s.

the Mori–Tanaka method. No shear correction factor is employed. Computed natural frequencies of the FG plate are found to match very well with their analytical values. Both for static and dynamic loads, the centroidal deflection of a FG plate is found to be between those for a pure ceramic and a pure metallic plate. The gradients in the material properties do not significantly affect the fundamental natural frequency of a simply supported square FG plate. Natural frequencies computed with a fifth order compatible shear and normal deformable plate theory, 169 uniformly distributed nodes on the midsurface of the square plate with length/thickness = 5 and the MLPG method are found to match very well with the analytical results. Thus the HOSNDPT and the MLPG method are effective in analyzing three-dimensional deformations of a thick plate.

Acknowledgements

This work was partially supported by the ONR's Research Program on Composites for Marine Structures under grant N00014-98-1-0300 to Virginia Polytechnic Institute and State University with Dr Y.D.S. Rajapakse as the Program Manager. L.F. Qian's work was also partially supported by the China Scholarship Council.

References

[1] Berger R, Kwon P, Dharan CKH. High speed centrifugal casting of metal matrix composites. The Fifth International Symposium on Transport Phenomena and Dynamics of Rotating Machinery, Maui, Hawaii; May 8–11, 1994.
[2] Fukui Y. Fundamental investigation of functionally gradient materials manufacturing system using centrifugal force. JSME Int J Ser III 1991;34:144–8.
[3] Choy K-L, Felix E. Functionally graded diamond-like carbon coatings on metallic substrates. Mater Sci Engng, A 2000;278:162–9.
[4] Khor KA, Gu YW. Effects of residual stress on the performance of plasma sprayed functionally graded ZrO_2/NiCoCrAlY coatings. Mater Sci Engng, A 2000;277:64–76.
[5] Lambros A, Narayanaswamy A, Santare MH, Anlas G. Manufacturing and testing of a functionally graded material. J Engng Mater Technol 1999;121:488–93.
[6] Breval E, Aghajanian K, Luszcz SJ. Microstructure and composition of alumina/aluminum composites made by the directed oxidation of aluminum. J Am Ceram Soc 1990;73:2610–4.
[7] Manor E, Ni H, Levi CG, Mehrabian R. Microstructure evaluation of SiC/Al_2O_3/Al alloy composite produced by melt oxidation. J Am Ceram Soc 1993;26:1777–87.
[8] Reddy JN. Analysis of functionally graded plates. Int J Numer Meth Engng 2000;47:663–84.
[9] Cheng ZQ, Batra RC. Deflection relationships between the homogeneous Kirchhoff plate theory and different functionally graded plate theories. Arch Mech 2000;52:143–58.
[10] Cheng ZQ, Batra RC. Exact correspondence between eigenvalues of membranes and functionally graded simply supported polygonal plates. J Sound Vib 2000;229:879–95.
[11] Cheng ZQ, Batra RC. Three-dimensional thermoelastic deformations of a functionally graded elliptic plate. Composites: Part B 2000;31: 97–106.
[12] Loy CT, Lam KY, Reddy JN. Vibration of functionally graded cylindrical shells. Int J Mech Sci 1999;41:309–24.
[13] Vel SS, Batra RC. Three-dimensional analysis of transient thermal stresses in functionally graded plates. Int J Solids Struct 2003; 40: 7181–96.
[14] Vel SS, Batra RC. Three-dimensional exact solution for the vibration of functionally graded rectangular plates. J Sound Vib 2004;272:703–30.
[15] Jin ZH, Batra RC. Some basic fracture mechanics concepts in functionally graded materials. J Mech Phys Solids 1996;44:1221–35.
[16] Jin ZH, Batra RC. Stress intensity relaxation at the tip of an edge crack in a functionally graded material subjected to a thermal shock. J Thermal Stresses 1996;19:317–39.

[17] Jin ZH, Batra RC. R-curve and strength behavior of a functionally gradient material. Mater Sci Engng 1998;A242:70–6.
[18] Batra RC, Vidoli S. Higher-order piezoelectric plate theory derived from a three-dimensional variational principle. AIAA J 2002;40: 91–104.
[19] Atluri SN, Shen SP. The meshless local Petrov–Galerkin (MLPG) method. Encino, CA: Tech Science Press; 2002.
[20] Atluri SN, Zhu T. A new meshless local Petrov–Galerkin (MLPG) approach in computational mechanics. Comput Mech 1998;22: 117–27.
[21] Qian LF, Batra RC, Chen LM. Elastostatic deformations of a thick plate by using a higher-order shear and normal deformable plate theory and two meshless local Petrov–Galerkin (MLPG) methods. Computer Model Engng Sci 2003;4:161–76.
[22] Qian LF, Batra RC, Chen LM. Free and forced vibrations of thick rectangular plates by using higher order shear and normal deformable plate theory and meshless local Petrov–Galerkin (MLPG) method. Computer Model Engng Sci 2003;4:519–34.
[23] Batra RC, Vidoli S, Vestroni S. Plane waves and modal analysis in higher-order shear and normal deformable plate theories. J Sound Vib 2002;257:63–88.
[24] Mori T, Tanaka K. Average stress in matrix and average elastic energy of materials with misfitting inclusions. Acta Metall 1973;21:571–4.
[25] Belytschko T, Lu YY, Gu L. Element-free Galerkin methods. Int J Numer Meth Engng 1994;37:229–56.
[26] Duarte CA, Oden JT. H-p clouds: an hp meshless method. Numer Meth Partial Differential Eq 2000;1–34.
[27] Liu W, Jun S, Zhang Y. Reproducing kernel particle method. Int J Numer Meth Engng 1995;20:1081–106.
[28] Lucy LB. A numerical approach to the testing of the fission hypothesis. Astronom J 1977;82(12):1013–24.
[29] Nayroles B, Touzot G, Villon P. Generalizing the finite element method: diffuse approximation and diffuse elements. Comput Mech 1992;20:307–18.
[30] Melenk JM, Babuska I. The partition of unity finite element method: Basic theory and applications. Computer Meth Appl Mech Engng 1996;139:289–314.
[31] Sukumar N, Moran B, Belytschko T. The natural element method in solid mechanics. Int J Numer Meth Engng 1998;43:839–87.
[32] Wendland H. Piecewise polynomial, positive definite and compactly supported radial basis functions of minimal degree. Adv Comput Meth 1995;4:389–96.
[33] Ching HK, Batra RC. Determination of crack tip fields in linear elastostatics by the meshless local Petrov–Galerkin (MLPG) method. Computer Model Engng Sci 2001;2(2):273–89.
[34] Batra RC, Ching HK. Analysis of elastodynamic deformations near a crack-notch tip by the meshless local Petrov–Galerkin (MLPG) method. Computer Model Engng Sci 2002;3:717–30.
[35] Lin H, Atluri SN. A meshless local Petrov–Galerkin (MLPG) method for convection diffusion problems. Computer Model Engng Sci 2002; 3(1):53–64.
[36] Long S, Atluri SN. A meshless local Petrov–Galerkin method for solving the bending problem of a thin plate. Computer Modeling Engng Sci 2002;3(1):53–64.
[37] Gu YT, Liu GR. A meshless local Petrov–Galerkin (MLPG) method for free and forced vibration analyses for solids. Comput Mech 2001; 27:188–98.
[38] Gu YT, Liu GR. A meshless local Petrov–Galerkin (MLPG) formulation for static and free vibration analyses of thin plates. Computer Model Engng Sci 2001;2:463–76.
[39] Mindlin RC, Medick MA. Extensional vibrations of elastic plates. J Appl Mech 1959;26:145–51.
[40] Lancaster P, Salkauskas K. Surfaces generated by moving least squares methods. Math Comput 1981;37:141–58.
[41] Chati MK, Mukherjee S. The boundary node method for three-dimensional problems in potential theory. Int J Numer Meth Engng 2000;47:1523–47.
[42] Newmark NM. A method of computation for structural dynamics. J Engng Mech Div, ASCE 1959;85:67–94.
[43] Fröhlich H, Sack R. Theory of the rheological properties of dispersions. Proc R Soc 1946;A185:415–30.
[44] Hill R. A self-consistent mechanics of composite materials. J Mech Phys Solids 1965;13:213–22.
[45] Jiang B, Batra RC. Effective properties of a piezocomposite containing shape memory alloy and inert inclusions. Continuum Mech Thermodyn 2002;14:87–111.
[46] Vel SS, Batra RC. Exact solution for thermoelastic deformations of functionally graded thick rectangular plates. AIAA J 2002;40: 1421–33.
[47] Vlasov BF. On one case of bending of rectangular thick plates. Vestnik Moskovskogp Universiteta, Serieiia Mate, Mekh, Astronom, Fiziki, Khimii 1957;2:25–34.
[48] Srinivas S, Rao AK, Rao CVJ. Flexure of simply supported thick homogeneous and laminated rectangular plates. Z Angew Math Mech 1969;49:449–58.
[49] Pagano NJ. Exact solutions for rectangular bidirectional composites and sandwich plates. J Compos Mater 1970;4:20–34.
[50] Batra RC, Geng TS. Enhancement of the dynamic buckling load for a plate by using piezoceramic actuators. Smart Mater Struct 2001;10: 925–33.
[51] Batra RC, Geng TS. Comparison of active constrained layer damping by using extension and shear mode actuators. J Intell Mater Struct 2002;13(6):349–67.
[52] Batra RC, Aimmanne S. Missing frequencies in previous exact solutions of free vibrations of simply supported plates. J Sound Vib 2003;265(4):887–96.
[53] Zhang GM, Batra RC. Modified smoothed particle hydrodynamics method and its application to transient problems, Comput Mech 2004. in press.
[54] Qian LF, Batra RC, Chen, LM. Analysis of cylindrical bending thermoelastic deformations of functionally graded plates by a meshless local Petrov-Galerkin method, Comput Mech 2004;33: 263–73.
[55] Qian LF, Batra RC. Design of bidirectional functionally graded plate for optimal natural frequencies, J Sound Vib. in press.
[56] Qian LF, Batra RC. Transient thermoelastic deformations of a thick functionally graded plate, J Thermal Stresses. in press.
[57] Batra RC, Jin J. Natural frequencies of a functionally graded anisotropic rectangular plate, J Sound Vib. in press.